Since January 2020 Elsevier has created a COVID-19 resource centre with free information in English and Mandarin on the novel coronavirus COVID-19. The COVID-19 resource centre is hosted on Elsevier Connect, the company's public news and information website.

Antiviral Research 174 (2020) 104697

Contents lists available at ScienceDirect

Antiviral Research

journal homepage: www.elsevier.com/locate/antiviral

In silico and *in vitro* analysis of small molecules and natural compounds targeting the 3CL protease of feline infectious peritonitis virus

Sirin Theerawatanasirikul[a], Chih Jung Kuo[b,**], Nanthawan Phetcharat[c], Porntippa Lekcharoensuk[c,d,*]

[a] Department of Anatomy, Faculty of Veterinary Medicine, Kasetsart University, Bangkok, 10900, Thailand
[b] Department of Veterinary Medicine, National Chung Hsing University, Taichung, 40227, Taiwan
[c] Department of Microbiology and Immunology, Faculty of Veterinary Medicine, Kasetsart University, 50th Ngamwongwan Rd., Ladyao, Chatuchak, Bangkok, 10900, Thailand
[d] Center of Advanced Studies in Agriculture and Food, KU Institute, Thailand

ARTICLE INFO

Keywords:
Feline infectious peritonitis virus (FIPV)
3CL protease
Natural compounds
Antiviral activity
Virtual screening
Coronavirus

ABSTRACT

The computational search of chemical libraries has been used as a powerful tool for the rapid discovery of candidate compounds. To find small molecules with anti-feline infectious peritonitis virus (FIPV) properties, we utilized a virtual screening technique to identify the active site on the viral protease for the binding of the available natural compounds. The protease 3CL ($3CL^{pro}$) plays an important role in the replication cycle of FIPV and other viruses within the family *Coronaviridae*. The 15 best-ranked candidate consensus compounds, based on three docking tools, were evaluated for further assays. The protease inhibitor assay on recombinant FIPV $3CL^{pro}$ was performed to screen the inhibitory effect of the candidate compounds with IC_{50} ranging from 6.36 ± 2.15 to 78.40 ± 2.60 μM. As determined by the cell-based assay, the compounds NSC345647, NSC87511, and NSC343256 showed better EC_{50} values than the broad-spectrum antiviral drug ribavirin and the protease inhibitor lopinavir, under all the test conditions including pre-viral entry, post-viral entry, and prophylactic activity. The NSC87511 particularly yielded the best selective index (> 4; range of SI = 13.80–22.90). These results indicated that the natural small-molecular compounds specifically targeted the $3CL^{pro}$ of FIPV and inhibited its replication. Structural modification of these compounds may generate a higher anti-viral potency for the further development of a novel therapy against FIP.

1. Introduction

Feline infectious peritonitis (FIP), caused by the virulent biotype of feline coronavirus (FCoV) of the genus *Alphacoronavirus* in the family *Coronaviridae*, is a progressive and fatal disease of cats. Feline infectious peritonitis virus (FIPV) is a mutated form of the parental enteric form of FCoV, called feline enteric coronavirus (FECV). FIPV infects domestic cats in multiple cat households worldwide (Manasateinkij et al., 2009; Pedersen, 2009, 2014a). FIP is a serious systemic (pyo-) granulomatous disease that causes protein-rich effusions in the body cavities. This disease progresses severely within a week to few months, before a cat dies (Pedersen, 2009). Several strategies have been used for supportive treatment against this disease. Anti-inflammatory and immunosuppressive drugs have been used to inhibit the inflammatory process and reduce the clinical signs with an aim to expand the life of a cat. The combination of antivirals and immuno-stimulating drugs has been applied for the treatment of coronaviruses in humans (Pedersen, 2014b). However, there is no report on the successful use of preventive vaccines and antiviral therapies to treat FIP.

The genome of FIPV contains a positive-sense, single-stranded RNA that is approximately 29,000 nucleotides in length, with 11 open reading frames (ORFs) encoding structural, non-structural, and accessory genes (Pedersen, 2009, 2014a; Lin et al., 2013). Two-thirds of the FCoV genome at the 5' end comprise two overlapping ORFs, ORF1a and 1b, which encode two polyproteins. The translation of ORF1a yields the polyprotein pp1a. At lower frequencies, ribosomes initiate translation at the beginning of ORF1a and undergo a frameshift at the junction between ORF1a and 1b, resulting in a long polyprotein, pp1ab

* Corresponding author. Department of Microbiology and Immunology, Faculty of Veterinary Medicine, Kasetsart University, 50th Ngamwongwan, Chatuchak, Bangkok, 10900, Thailand.
** Corresponding author. Department of Veterinary Medicine, National Chung Hsing University, 145 Xingda Rd. Taichung, 40227, Taiwan.
E-mail addresses: ck476@nchu.edu.tw (C.J. Kuo), fvetptn@ku.ac.th (P. Lekcharoensuk).

https://doi.org/10.1016/j.antiviral.2019.104697
Received 28 September 2019; Received in revised form 15 December 2019; Accepted 16 December 2019
Available online 18 December 2019
0166-3542/

(Pedersen, 2014a; St. John et al., 2015; Wang et al., 2015). Similar to other coronaviruses (CoV), FCoV pp1ab contains two cysteine proteases, the papain-like protease (PL^{pro}) and the 3-chymotrypsin-like protease ($3CL^{pro}$). The $3CL^{pro}$ is also known as the main protease (M^{pro}) (Pedersen, 2014a; St. John et al., 2015; Wang et al., 2015; Berry et al., 2015) that plays a pivotal role in the viral life cycle, including the processing of polyprotein and viral replication. The polyprotein pp1a and pp1ab are subsequently enzymatically cleaved into 16 nonstructural functional proteins (nsp1 to nsp16) that are mainly involved in proteolytic processing and viral RNA synthesis, including the replication of the genome and synthesis of the sub-genomic mRNA. The remaining genome contains nine ORFs that encode four structural proteins—spike (S), nucleocapsid (N), membrane (M), and envelope (E) proteins, and five accessory proteins (3a–c, 7a, and 7b).

The $3CL^{pro}$ of CoV has similar structural and functional properties as the 3CL protease or $3CL^{pro}$ of picornavirus, norovirus, and SARs-CoV (Kim et al., 2013). In human CoV, the $3CL^{pro}$ has been termed "the Achilles' heel of coronaviruses". It is an attractive target for drug discovery. The $3CL^{pro}$ of FIPV could act as a model to study the potential antiviral drugs against further emerging CoV-associated diseases. The *in vitro* assay is particularly available in the FIPV system. The inhibitors that target $3CL^{pro}$, including pyridine N-oxide derivatives, peptidomimetic analogs, covalent inhibitors, and peptidyl compounds, have been evaluated previously (Balzarini et al., 2006; Kim et al.; 2012, 2013; Berry et al., 2015). Natural products from herbal extracts could represent a major resource for the development of antiviral drugs. Previous studies have shown that natural compounds exhibit antiviral activities against the $3CL^{pro}$ of SARs-CoV and interfere with viral replication (Lin et al., 2005; Ryu et al., 2010). An antiviral drug targeting the $3CL^{pro}$ is not yet available.

In this study, we utilized an *in silico* approach to search for the candidate anti-FIPV lead compounds from the available database, particularly, natural compounds targeting the FIPV $3CL^{pro}$. This approach could circumvent major investments on agents or drugs that do not present suitable properties and reduce the chances of failure of downstream *in vitro* and *in vivo* assays as well as during the later stages of clinical tests. In addition, the compounds identified by this method may provide useful precursors and information for the further development of potential therapeutic agents against FIP and other emerging CoV-associated diseases.

2. Materials and methods

2.1. Preparation of FIPV–$3CL^{pro}$ structure and natural compound library

The crystal structure of $3CL^{pro}$ was obtained from the Protein Data Bank (PDB) (ID: 5EU8). This structure was processed to prepare it for the molecular docking studies. This preparation involved adding hydrogen atoms, eliminating water molecules, removing some ions, specifying the correct protonation and tautomerization states of the binding site residues, and calculating the partial charge using the program Chimera (UCSF, San Francisco, USA). The prepared structures were saved as pdb and mol2 files for subsequent molecular docking analysis. A total of 8,338 structural files of natural compounds were retrieved from PubChem, Drugbank, Zinc, and NCI databases to generate a library of initial compounds for the screening process. The structures of the compounds were saved in mol2 and sdf formats prior to the docking analysis.

2.2. Virtual screening analysis

Initial virtual screening studies were carried out using the program AutoDock Vina (Trott and Olson, 2010), which was built into the PyRx suite (version 0.9.7) to evaluate the empirical scoring function of the ligand-protein complex (Dallakyan and Olson, 2015). The input files were converted to the pdbqt file format. The grid parameters were grid center (x = −40, y = −10, z = −5) and size (x = 30, y = 30, z = 30), wherein the space was at the center of the catalytic pocket of FIPV $3CL^{pro}$. Lamarckian genetic algorithm (GA) was set by default, where the parameters included 20 GA runs, 150 individuals in the population, and 270,000 generations. The top 10 outputs of the best binding affinities for each docking run were stored. In this study, the 64 selected compounds were re-scored using different docking algorithms on the program GOLD version 5.5 (license kindly provided by Assoc. Prof. Dr Kiattawee Choowongkomon, Kasetsart University), based on GA. The grid parameters of the interface region were similar to those set for PyRx with 20 GA runs. The score function was based on the GoldScore fitness function for ranking of the binding affinity. The second program for re-scoring, ICM-pro suite version 3.8.6, was used to calculate energy according to the Monte Carlo biased-probability algorithm. The grid space was adjusted similarly for both the mentioned software. The parameters of Receiver Operating Characteristic (ROC) curves and Areas Under the ROC Curve (AUCs) were applied to determine the performance of each scoring function and docking performances. The interactions of protein-ligand complexes were characterized using the program LigPlot version 1.4.5. (Laskowski and Swindells, 2011) and the structural complexes were visualized using the UCSF Chimera version 1.10.2 (UCSF, San Francisco, USA). The ADME/T (Absorption, Distribution, Metabolism, Elimination, and Toxicity) analysis was subsequently performed on the selected candidate compounds using the web-based software SwissADME (Daina et al., 2017) and OSIRIS DataWarrior version 5.0 (Sander et al., 2015).

2.3. Expression and purification of FIPV–$3CL^{pro}$

The gene encoding FIPV–$3CL^{pro}$ was amplified from the cDNA of FIPV strain 79–1146 (ATCC, VR–990) with forward primer (5′-CATGC CATGGCT*ATCGAGGGAAGG*TCCGGATTGAGAAAAATGGCAC–3′) containing an *Nco*I site (underlined) and an FXa protease cleavage site (Ile-Glu-Gly-Arg, italicized), and reverse primer (5′-CCGCTCGAGTTACTG AAGATTAACACCATACATTTGC–3′) containing an *Xho*I site (underlined). The PCR product was digested using *Nco*I and *Xho*I, and then ligated into a pET32a vector. The recombinant protease plasmid was then used to transform *E. coli* DH5α-competent cells that were then streaked on a Luria-Bertani (LB) agar plate containing 100 μg/mL ampicillin. Ampicillin-resistant colonies were selected from the agar plate and cultured in 5 mL of LB broth containing 100 μg/mL ampicillin overnight at 37 °C. The correct constructs were subsequently transformed to *E. coli* BL21 (DE3) for protein expression. The 5-mL overnight culture of a single transformant was used to inoculate 500 mL of fresh LB medium containing 100 μg/mL ampicillin. The cells were grown to the appropriate optical density (OD_{600} = 0.6) and induced with 1 mM Isopropyl- β-D-1 thiogalactopyranoside. After 4–5 h, the cells were harvested by centrifugation at 7,000 × *g* for 15 min. The protein purification was carried out as described previously (Kuo et al., 2004). Briefly, the gene encoding FIPV $3CL^{pro}$ was amplified using PCR and inserted into the commercial vector pET32a for the expression of the enzyme with thioredoxin, hexa-His tag, and a cleavage site for FXa protease on the N-terminus. After cleavage of the tag by FXa protease, the mixture was loaded onto another Ni-NTA column to remove the thioredoxin and hexa-His tag. The purity of the tag-free FIPV $3CL^{pro}$ was evaluated using SDS-PAGE. The protein having a purity of more than 90% was first dialyzed in a buffer containing 12 mM Tris-HCl (pH 7.5), 120 mM NaCl, 0.1 mM EDTA, 7.5 mM β-mercaptoethanol, and 1 mM dithiothreitol (DTT), and then subjected to the next experiment.

2.4. Examination of the enzymatic activity and inhibition assay of protease

The kinetic measurements of FIPV $3CL^{pro}$ were carried out following the previously described procedures (Kuo et al., 2004). FIPV $3CL^{pro}$ was added to a solution containing 20 mM Bis-Tris (pH 7.0) at 25 °C. Enhanced fluorescence resulting from the cleavage of the fluorogenic

substrate peptide (Dabcyl-KTSAVLQSGFRKME-Edans) of FIPV $3CL^{pro}$ was monitored at 538 nm (Dabcyl), with excitation at 355 nm (Edans), on a fluorescence plate reader (BMG FLUOstar OPTIMA Microplate Reader, Ortenberg, Germany). The concentration of FIPV $3CL^{pro}$ that was used to measure *K*m and k_{cat} values was 35 nM, while the substrate concentrations were ranged from 0.5 to 5-fold of the *K*m value. The initial rate up to 10% substrate consumption was used to calculate the kinetic parameters using the Michaelis-Menten equation on the program KaleidaGraph. For the protease inhibition assay, the initial rates of inhibition of 35 nM enzyme using 6 μM fluorogenic substrate were plotted against different inhibitor concentrations to obtain the IC_{50} values. The K_i measurements were performed at two fixed inhibitor concentrations of 1- and 2-fold of IC_{50}. Substrate concentrations ranged from 3 to 40 μM in a reaction mixture containing 35 nM FIPV $3CL^{pro}$. Lineweaver-Burk plots of kinetic data were fitted using nonlinear regression on the computer program KinetAsyst II (IntelliKinetics, State College, PA), to obtain the K_i value for competitive inhibitors using Eq. (1).

$$1/V = K_m/V_m\,(1+[I]/K_i)1/[S] + 1/V_m \quad (1)$$

In this equation, K_m is the Michaelis-Menten constant of the substrate, K_i is the inhibition constant, V_m is the maximal velocity, and [I] and [S] represent the inhibitor and substrate concentrations in the reaction mixture, respectively.

2.5. Growth of the virus in cell culture

The Crandell-Rees feline kidney (CRFK) cell line (ATCC, CCL–94) was used for viral propagation and titration. The cell lines were maintained in Modified Eagle Medium (MEM, Invitrogen™, Carlsbad, USA), supplemented with 7% fetal bovine serum (FBS, Invitrogen™, Carlsbad, USA), 2 mM L-glutamine (Invitrogen™, Carlsbad, USA) and Antibiotic-Antimycotic (Invitrogen™, Carlsbad, USA). The CRFK cell lines were inoculated with FIPV strain 79–1146 (ATCC, VR–990) and incubated at 37 °C with CO_2 for 48 h. The cytopathic effect (CPE) was observed by an inverted microscope (Olympus CKX41, Tokyo, Japan). The infected cells were subjected to a double freeze/thaw cycle to release cell-bound viruses. The virus suspension was clarified by centrifugation at 2,000 × *g* for 10 min at 4 °C. The clear supernatant was collected and kept at −80 °C until used.

2.6. Cytotoxicity assay

The CRFK cells were seeded at 1×10^5 cells/mL (100 μL/well) onto a 96-well plate and incubated overnight. On the following day, the cells were incubated with varying concentrations (200, 100, 10, 1 and 0.1 μM) of the test compounds for 48 h. Three independent experiments were performed to test the cytotoxicity. To determine the population of living cells, 20 μL of MTS solution (CellTiter 96 Aqueous Non-radioactive Cell Proliferation Assay Kits, Promega®, Madison, USA) was added into each culture well. The MTS tetrazolium compound was bioreduced by the metabolically active cells into formazan as a product, which turned the media to yellow. The color intensity was proportional to the number of living cells. After incubation at 37 °C for 2 h, the optical density of each sample was measured at 490 nm using a multimode reader (Synergy H1 Hybrid Multi-Mode Reader, BioTek®, USA). The absorbance values of the compound treated wells were divided by the average of the absorbance of the control wells. The ratio of inhibition was calculated as 50% cytotoxicity (cytotoxic concentration; CC_{50}) using nonlinear regression analysis. The results were presented as means and standard deviation using the statistical software Prism version 5.0.1 (GraphPad, San Diego, USA).

2.7. Antiviral assay

Antiviral activities of the candidate compounds were examined using CRFK cells infected with different concentrations of FIPV with two biological and three technical replicates. The CRFK cells were seeded at 1×10^5 cells/mL (100 μl/well) onto a 96-well plate for the immunoperoxidase monolayer assay (IPMA), and at 5×10^4 cells/well into a 24-well plate for qPCR-based detection of the virus. The inhibitory activities of each compound at all the tested concentrations were compared with ribavirin, a broad-spectrum antiviral drug, and lopinavir, an HIV-protease inhibitor, as positive control drugs, for 24 h. A set of wells designated as negative control, consisting of no inhibitor with 1% DMSO control, no virus control, and no inhibitor or virus control, was included in each experiment. Three conditions were generated for each tested compound.

2.7.1. Pre-viral entry activity

To determine the inhibitory activities of the compounds against FIPV $3CL^{pro}$ before the entry of the virus into the host cells, the CRFK cells were incubated overnight as mentioned above. The FIPV strain 79–1146 at 100 units of 50% Tissue Culture Infective Dose ($TCID_{50}$) was inoculated simultaneously with different concentrations of each compound into separate wells. The final concentrations of each compound were 100, 50, 20, 10, 5, 1, and 0.5 μM per well, based on the CC_{50} values obtained from the cytotoxicity assay. The cells were incubated at 37 °C for 24 h.

2.7.2. Post-viral entry activity

In order to determine the antiviral activities of the candidate compounds against intracellular replication of FIPV, CRFK cells were inoculated with FIPV at 100 $TCID_{50}$/well. The infected cells were incubated at 37 °C for 2 h for viral adsorption. Then, the infected-CRFK cells were incubated for 24 h with different concentrations of each compound as mentioned above.

2.7.3. Prophylactic activity

In order to determine whether small molecules could enter the host cells and demonstrate antiviral activity after FIPV infection, the CRFK cells were incubated with the candidate compounds prior to viral inoculation. The seeded CRFK cells were first incubated overnight, following which they were incubated with different concentrations of the compounds at 37 °C for 2 h. The compound solution was then removed and the cells were washed once with Ringer's saline solution (pH 7.4). Then, the cells were inoculated with FIPV at 100 $TCID_{50}$/well and incubated at 37 °C for 24 h.

2.8. Detection of FIPV antigens using immunoperoxidase monolayer assay (IPMA)

IPMA was performed using a previously described method (Lekcharoensuk et al., 2012). Briefly, the infected CRFK cells were fixed with cold methanol at room temperature for 20 min and then washed with PBST buffer. The primary antibody for detection of FIPV, a mouse monoclonal antibody specific to pan-coronavirus FIPV3–70 (dilution 1:500, ThermoFisher, Carlsbad, USA), was incubated with the infected cells at 37 °C for 1 h. These treated cells were then washed using PBST, following which they were incubated with the secondary antibody, a goat anti-mouse IgG-HRP antibody (dilution 1:400, Kirkegaard & Perry Laboratories, Madison, USA), at 37 °C for 1 h. The antigen-antibody reaction was stained using DAB substrate (DAKO, Santa Clara, USA) and observed under a phase-contrast inverted microscope (Olympus CKX41, Tokyo, Japan).

2.9. Image analysis

The antiviral activities of the tested compounds were evaluated by

measuring the intensity and numbers of the positive FIPV-infected CRFK cells using IPMA assay. Five concentrations of each compound were added to 96-well plates in duplicate. Images of the presenting FIPV antigens in the infected cells were analyzed using the software CellProfiler (version 2.7.0), with an open-source code of available algorithms (Broad Institute; freeware available at http://www.cellprofiler.org/index.htm). Five images from each concentration of the tested compounds were used for the analysis. The CellProfiler pipeline that was utilized in this project was modified from the open-source (https://forum.image.sc). The pipeline, IPMA1.cppippe, was developed to calculate the intensity of the DAB-stained cell parts compared to the unstained cell parts, and set to separate clumped from isolated cells based on their shapes.

Under three antiviral conditions, an active compound or "hit" is a compound that exhibits at least 50% inhibition of positive FIPV-infected cells without compromising cell viability. The effective concentration at which the compound inhibited 50% of the infected cells (EC_{50}) in the absence of drug was determined. The selectivity index (SI) was calculated as SI = CC_{50}/EC_{50}.

2.10. Viral quantification using real-time qPCR

The RNA was extracted from supernatants of each sample. Viral RNAs were extracted using the Trizol Total RNA extraction kit (Invitrogen™, Carlsbad, USA) according to the manufacturer's instructions. The RNA was reverse transcribed into cDNA which in turn was the template for the following real-time quantitative polymerase chain reaction (qPCR). Quantitative amplification and melting curve analysis were carried out by real-time qPCR (C1000 Touch Thermal Cycler, Bio-Rad, USA). Two FIPV-specific primers were used for the quantification of its nucleic acid. The primers for FIPV-PCR that targeted the 3′-untranslated region (3′-UTR) of ORF7ab were used for the amplification (Herrewegh et al., 1995; Manasateinkij et al., 2009). The sequences of primers specific to the FCoV viral genome were: 5′-GGCAACCCGATG TTTAAAACTGG-3' (upstream; nucleotides 1 to 23) and 5′-CACTAGAT CCAGACGTTAGCTC-3' (downstream; nucleotides 211 to 192). The reaction mixture for qPCR was prepared using SsoFast EvaGreen Supermix (2x) (Bio-Rad, Hercules, USA) and the cycling conditions were set according to the manufacturer's protocol. The qPCR amplification for each sample was carried out in duplicate. The standard curve was generated by ten-fold serial dilution (10^{-2} to 10^{-7}) of plasmid containing the FIP 3′-UTR sequence. The linear part of the amplification curves was plotted against the log values of the starting concentrations, which yielded $r^2 \geq 0.99$. The Cq values were then automatically generated using the software CFX Maestro™ (Bio-Rad, Hercules, USA). The absolute quantities of viral copy numbers were calculated for each treatment and control. The antiviral activities of the selected candidate compounds were presented as percent viral reduction by each compound compared to the control, and validated by three independent experiments.

3. Results

3.1. Molecular docking of FIPV $3CL^{pro}$

Molecular docking analyses were initially carried out using the program Autodock Vina, and then re-docked using the GOLD and ICM-pro programs. The candidate compounds were ranked according to the affinity-binding scores, and then the consensus scores were used to narrow down their hits (Supplementary Table 1). The AUC value can discriminate between the sensitivity and specificity of a set of docked results from individual scoring functions. Our validation dataset consisted of 64 compounds, which was sufficient for the analysis. The results showed a significantly higher AUC (0.886) of three, rather than two, combinations of the scoring functions (Fig. 1). The fifteen selected compounds demonstrated strong interactions in the FIPV $3CL^{pro}$ binding pocket, which was suitable for further assays.

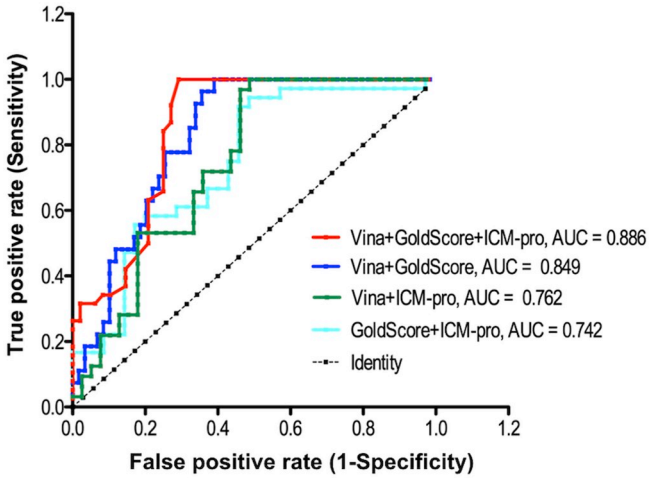

Fig. 1. Consensus scorings of three docking tools for the FIPV $3CL^{pro}$ validation dataset.

3.2. Protein purification and inhibition of FIPV $3CL^{pro}$

Recombinant his-tagged FIPV $3CL^{pro}$ that was expressed in *E. coli* BL21 (DE3) was subsequently purified by the Ni-NTA column. Following proteolytic cleavage with FXa protease, the tag-free FIPV 3CLpro with high purity was shown on the SDS-PAGE (Fig. 2A). Since extra residues or hexa-His tags at the N- or C-terminus have been demonstrated to interfere with the dimerization of SARs $3CL^{pro}$ (Hsu et al., 2005), the tag-free FIPV $3CL^{pro}$ prepared in this study should reflect the actual activity. Moreover, owing to its high degree of homology to SARS $3CL^{pro}$, the enzyme kinetic analysis was performed by using the same fluorogenic substrate (Dabcyl-KTSAVLQSGFR-KME-Edans) as described previously (Kuo et al., 2004). The K_m value of FIPV $3CL^{pro}$ was measured to be 8.56 ± 1.15 μM, and the k_{cat} value was 0.71 ± 0.04 s^{-1} (Fig. 2B).

Fifteen compounds selected by the molecular docking analysis were subsequently tested using the inhibition assay against FIPV $3CL^{pro}$. During the primary screening, seven compounds showed more than 50% inhibition of the enzyme activity at a concentration of 100 μM (Table 1). The seven hits NSC345647, NSC87511, NSC343256, CID5318214, CID3821945, CID5748601, and CID5372747 displayed IC_{50} values of 6.3 ± 2.1 μM, 29.4 ± 4.6 μM, 24.5 ± 8.9 μM, 28.5 ± 4.2 μM, 10.3 ± 2.5 μM, 77.2 ± 13.8 μM, and 78.4 ± 2.6 μM, respectively. The K_i values of these seven compounds against FIPV $3CL^{pro}$ were 3.6 ± 0.3 μM (NSC345647), 17.0 ± 1.8 μM (NSC87511), 11.7 ± 0.9 μM (NSC343256), 16.7 ± 1.7 μM (CID5318214), 5.8 ± 0.7 μM (CID3821945), 45.2 ± 3.6 μM (CID 5748601), and 48.8 ± 4.1 μM (CID5372747), indicating that these compounds were competitive inhibitors. However, the compounds CID452967, NSC14975, NSC38273, NSC142227, CID71313853, NSC36398, NSC270914, and NSC131547 did not show any significant inhibition, with IC_{50} values greater than 500 μM. The IC_{50} and K_i values of all the tested compounds are summarized in Supplementary Table 1.

3.3. Cytotoxicity of the natural compounds

The cytotoxicity assay revealed that five of the seven hits showed 50% cytotoxicity (50% cell cytotoxicity, CC_{50}) at concentrations higher than 300 μM. The CC_{50} values of compounds NSC87511, CID5318214, CID3821945, CID5748691, and CID5373747 were higher than their IC_{50} values (Supplementary Table 1). Generally, if the IC_{50} of a compound is less than the CC_{50}, the compound can effectively inhibit the virus without exhibiting significant cell toxicity.

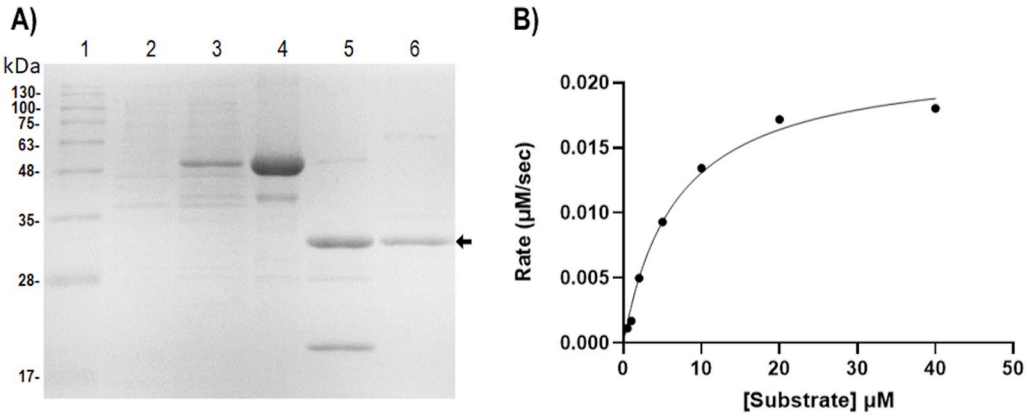

Fig. 2. Protein purification and kinetic parameters of FIPV 3CL^{pro}. (A) SDS-PAGE analysis of the FIPV 3CL protease at different stages of the purification procedure. Lane 1 represents the molecular mass markers. Lanes 2 and 3 show the cell lysate without and with IPTG induction to overexpress FIPV 3CL protease with fusion tag, respectively. Lane 4 is the tagged protease after Ni-NTA column chromatography. Lane 5 represents the purified FIPV 3CL^{pro} after cleavage of FXa to remove the fusion tag. Two extra bands of the intact FIPV 3CL^{pro} and the fusion tag at lower molecular mass appear on SDS-PAGE. Lane 6 shows the purified untagged protease (arrowed) after passing the second Ni-NTA column. (B) Determining the kinetic parameters of FIPV 3CL protease. The initial reaction rates of the protease at different substrate concentrations were plots against substrate concentrations to obtain the V_{max} and K_m values of the enzyme. GraphPad Prism software was used to fit the kinetic data using Michaelis-Menten equation. The k_{cat} and K_m of this reaction were 0.71 ± 0.04 s^{-1} and 8.56 ± 1.15 μM, respectively.

3.4. Antiviral activities of the natural compounds

We evaluated the viral infection based on differential expression of the FIPV antigens within the cytoplasm of mock- and virus-infected CRFK cells. The antiviral activity before the entry of the virus into the host cell was determined to check if the compounds could inhibit the virus at this stage. The compounds NSC345647, NSC87511, and NSC343256 demonstrated more effective inhibitory activity than ribavirin. Furthermore, the compounds NSC345647 and NSC343256 showed better EC_{50} values than the reference protease inhibitor (lopinavir). The same compounds were also observed to inhibit FIPV replication in CRFK cells during the post-viral entry step of FIPV infection when FIPV 3CL^{pro} was also expressed by the viral gene. The results indicated that three compounds had the better EC_{50} values. The prophylactic or protective activity was determined to check if the compounds could penetrate the host cells and still possess the inhibitory activity to prevent FIPV infection. The results revealed that the compounds NSC345647, NSC87511, and NSC343256 could completely protect the cells from virus infection at concentrations of 20–50 μM. However, the remaining compounds could not inhibit FIPV infection in any of these conditions, despite having good IC_{50} values. The compound NSC87511 showed high SI values (> 4.00) in all the three conditions (Table 1). The qPCR results showed that the percentage of viral reduction by the selected compounds in all the three conditions mostly corroborated with the IPMA results (Figs. 3 and 4).

3.5. Protein-ligand interaction

The protease-inhibition and antiviral activity assays demonstrated that three compounds possessed anti-FIPV activities. Therefore, we further analyzed the interactions between the compounds and the active site of 3CL^{pro}, especially those between the key amino acid residues. All the compounds were firmly placed within the binding pocket of FIPV 3CL^{pro}, where the catalytic residues His41 and Cys144 were present. The binding pockets of FIPV 3CL^{pro} exhibited non-covalent interactions with the small molecules (Fig. 5), which is favorable in drug design. The non-covalent interactions between amino acid residues in the binding pocket of FIPV 3CL^{pro} and each compound are detailed as follows: 1) compound NSC345647 (upper panel A, alkyl/π-alkyl: His41, Cys144, Pro188; π-donor: Glu165; lower panel A, hydrophobic interaction: Thr47, Phe139, Ala141, His163; hydrogen bond: Ile140, Gly142, Cys144, Glu165); 2) compound NSC87511 (B upper panel, alkyl/π-alkyl: His163, Leu164, Pro188; π-sigma: His41; lower panel B, hydrophobic interactions: Cys144, Asp186, Gln187; hydrogen bond: Thr47, Glu165); compound NSC343256 (upper panel C, Alkyl/π-alkyl:Cys144, Pro188; π-π stacking: His41; hydrogen bond:THR47; lower panel C, hydrophobic interactions: Asn25,

Table 1
The selected-candidate compounds with CC_{50} and EC_{50} values from the cell-based assays.

no.	Compound ID	Cell-based assay[b]						
		Cytotoxicity CC_{50} (μM)[a]	Pre-viral entry (EC_{50}; μM)[c]		Post-viral entry (EC_{50}; μM)[d]		Prophylactic antiviral activity (EC_{50}; μM)[e]	
			IPMA	SI	IPMA	SI	IPMA	SI
1	NSC345647	10.53 ± 0.13	1.19 ± 0.95	8.88	4.867 ± 0.12	2.20	2.851 ± 0.520	3.69
2	NSC87511	371.90 ± 0.26	16.24 ± 1.33	22.90	21.83 ± 1.64	17.04	26.94 ± 1.25	13.80
3	NSC343256	56.87 ± 0.73	3.83 ± 0.44	2.89	4.00 ± 0.37	2.77	16.22 ± 1.23	0.68
4	CID5318214	339.30 ± 0.03	> 100	N/A	> 100	N/A	> 200	N/A
5	CID3821945	306.8 ± 0.175	> 100	N/A	> 100	N/A	> 200	N/A
6	CID 5748601	425.30 ± 0.13	> 100	N/A	> 100	N/A	> 200	N/A
7	CID5372747	336.20 ± 0.13	> 100	N/A	> 200	N/A	> 200	N/A
Ribavirin	CID37542	> 500	48.87 ± 1.77	25.68	73.98 ± 0.18	16.96	> 200	N/A
Lopinavir	CID92727	> 500	8.56 ± 0.47	61.52	5.38 ± 2.32	97.83	31.70 ± 1.37	16.61

ND not determined.
[a] Fifty percent of cytotoxic concentration (CC_{50}) by MTS assay.
[b] The results show three independent cell-based assays to determine the effective concentration (EC_{50}) using MTS and IPMA assays; Selectivity index (SI) = CC_{50}/EC_{50}.
[c] 100 $TCID_{50}$ FIPV incubation with compounds.
[d] 100 $TCID_{50}$ FIPV adsorption at 37 °C for 2 h before adding the tested compounds.
[e] Compound incubation at 37 °C for 2 h, before inoculation with FIPV at 100 $TCID_{50}$/well.

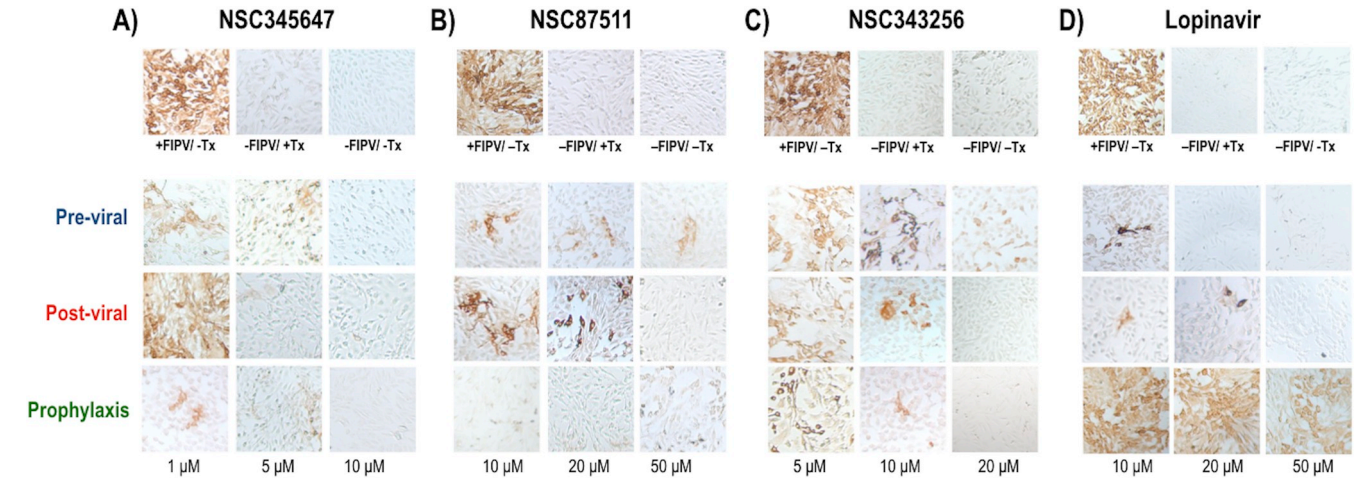

Fig. 3. Antiviral activities of the best three compounds as detected by IPMA, NSC345647 (A), NSC87511 (B), and NSC343256 (C). Lopinavir (D), an HIV-protease inhibitor, was included as a positive drug control. Three controls for each compound (FIPV infection without the compound treatment, FIPV ± Tx; no infection with compound, -FIPV/ + Tx; no infection without compound, -FIPV/-Tx) are presented on the upper panel. The three-antiviral cell-based conditions; pre-viral entry, post-viral entry, and prophylaxis activities are presented as described in the text.

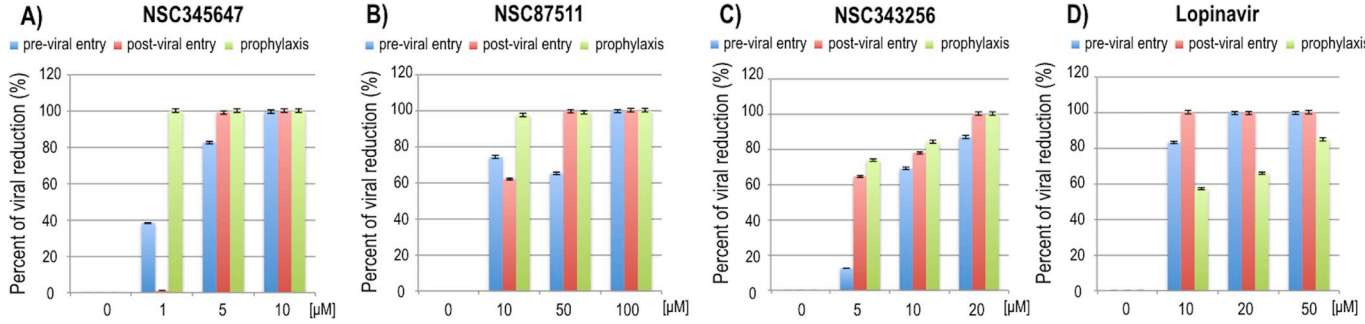

Fig. 4. Real-time qPCR (A–D) demonstrating percent of viral reduction in the FIPV-infected CRFK cells after being treated with each compound in three antiviral cell-based conditions; pre-viral entry, post-viral entry, and prophylaxis activities as described in the text. The reductions of viral copy numbers were related to that of FIPV-infected CRFK cells in the absence of any compounds.

Glu118, His163, Leu164, Asp186, Gln187; hydrogen bonds: Asn24, Val26, Thr47). In particular, all the compounds showed interactions with the thiol group of cysteine (Cys144) and the imidazole ring of histidine (His41) (Fig. 5). In addition, we evaluated the drug-like physicochemical properties of the candidate compounds using the Lipinski's Rule of Five (Rule-of–5, Ro5; Lipinski, 2004) and ADME/T properties. The Ro5 criteria defined four ranges of simple physicochemical parameters, molecular weight ≤500, log P ≤ 5, H-bond donors ≤5, and H-bond acceptors ≤10, which are mostly associated with orally active drugs. The compounds NSC87511 and NSC343256 abided by the 'drug-likeness' criteria, except the compound NSC345647, which showed less potential for orally-active properties (Supplementary Table 2). None of the compounds possessed significant mutagenic or irritant properties.

4. Discussion

In this study, we generated recombinant $3CL^{pro}$ of FIPV carrying nonredundant residues at both N- and C-termini. This is the first report to describe the kinetic characteristics of tag-free FIPV $3CL^{pro}$ using the fluorogenic substrate, which displayed the k_{cat} and Km of 0.71 ± 0.04 s-1 and 8.56 ± 1.15 μM, respectively. By taking advantage of structure-based virtual screening, three candidate compounds, NSC345647, NSC87511, and NSC343256, were shown to possess antiviral activity. The compound NSC345647 was a fungal metabolite called Chaetochromin, isolated from *Fusarium* (Ascomycotina, Hypocreales), *Penicillium, Chaetomium,* etc. Chaetochromin A is a symmetrical dimer having two trans-2,3-dimethyl groups on the 5,6,8-trihydroxy-naphtho-γ-pyrone ring (Ugaki et al., 2012). Chaetochromin and their derivatives have been reported as inhibitors of HIV integrase, based on strand-transfer assay of recombinant integrase, with IC_{50} = 1–12 μM (Singh et al., 2003). Using *in silico* analysis, the complex of chaetochromin and HRAS protein in AIDS-associate cancers was simulated, and chaetochromin B was observed to be stable in the binding pocket, making it a promising antiviral drug (Omer and Singh, 2017). In our study, the three viral infection assays showed that chaetochromin could inhibit FIPV infection, with low IC_{50} and EC_{50}. However, it might have a cytotoxic effect on the host cells *in vivo*.

Stictic acid (NSC87511) was an extract from species of lichens (*Usnea articulata*, *Lobaria pulmonaria*, *Xanthoparmelia conspersa*, *Xanthoparmelia camtschadalis,* and *Hypotrachyna revoluta*) (White et al., 2014). Stictic acid is a β-orcinol depsidone that is produced by the lichens. The polyketides and their unique secondary metabolites containing aromatic rings are commonly found in stictic acid. The derivatives of stictic acid could reduce the production of reactive oxygen species (ROS) in the cells via their anti-oxidative activity (Lohézic-Le Dévéhat et al., 2007; Papadopoulou et al., 2007). Moreover, stictic acid could react with the Cys141 within the cysteine triad of tumor suppressor protein p53, to reduce its reactivation in human cancers (Wassman et al., 2013). It should be noted that $3CL^{pro}$ of CoV also contains cysteine as the nucleophilic active site in the catalytic dyad (Cys144 and His41) (Kuo et al., 2004; Kim et al., 2012). In our docking study, the compound interacted with His41 (hydrophobic bond) and Cys144 (hydrophobic and hydrogen bonds). We also observed the protease-inhibitory effect of NSC87511 (Supplementary Table 1) during the FIPV $3CL^{pro}$ inhibition assay. Stictic acid derivatives and atranorin that were extracted from

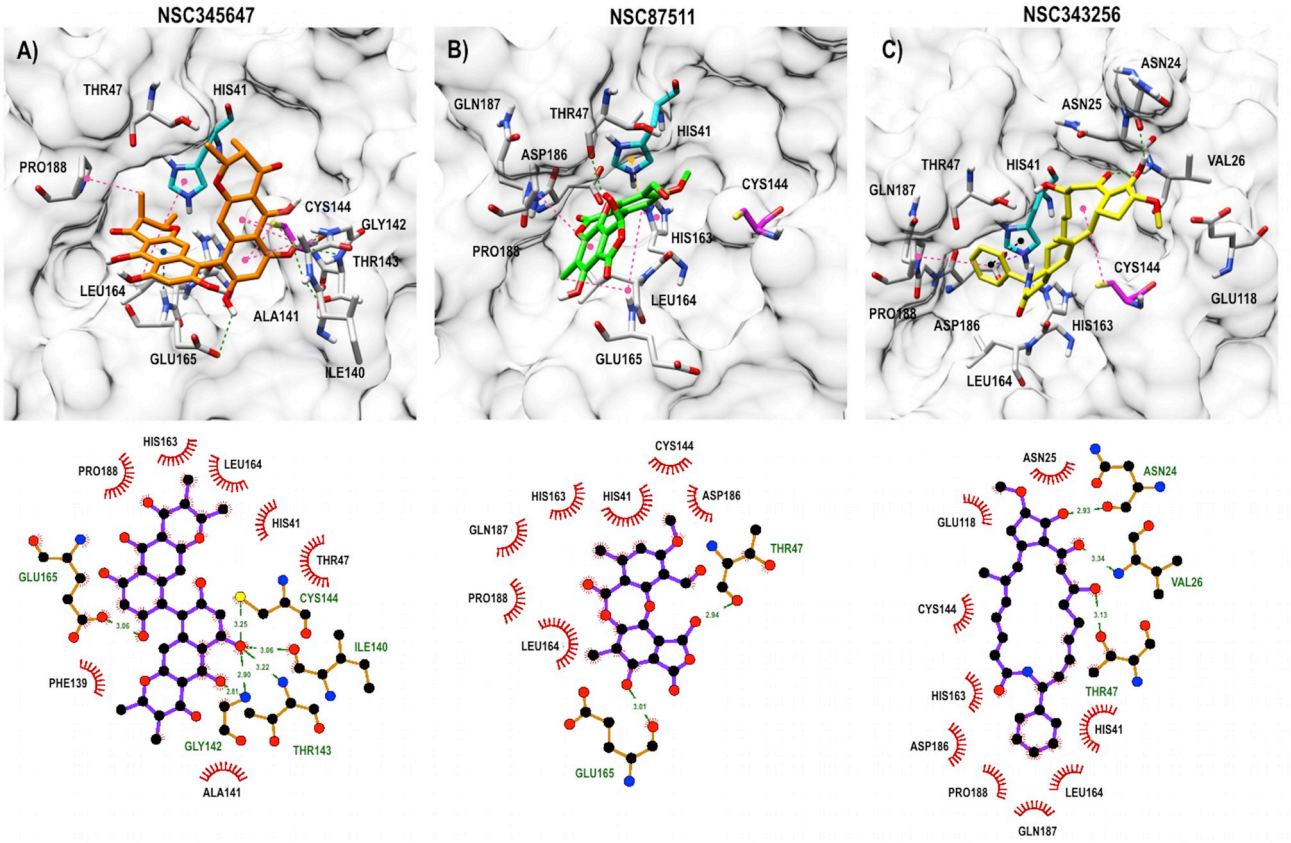

Fig. 5. FIPV 3CL^{pro} – The interactions with three compounds with high affinity. A) NSC345647, B) NSC87511 and C) NSC343356 are docked in 3D-structures (upper panel) and 2D-structures (lower panel) at the substrate-binding pocket of FIP 3CL^{pro}. The interactions are presented as dashed lines for alkyl/π-alkyl bonds (pink), π-donor (dark blue), π-π stack (black), π-sigma (yellow), π-cation (purple), hydrogen bonds (green) and hydrophobic interaction (red circles and ellipses). The ligand-protein interactions are visualized using UCSF Chimera version 1.10.2 and LigPlot software.

lichens using acetone could inhibit the replication of hepatitis C virus (Vu et al., 2015). In addition, the stictic acid also exhibited anti-HIV-1 integrase activities, with IC_{50} < 50 μM (Neamati et al., 1997).

Hitachimycin (NSC343256), a natural compound, was first isolated from *Streptomyces scabriporus* (Umezawa et al., 1981). It was also known as stubomycin, which is one of the β-amino acid-containing macrocyclic lactam polyketides, with β–phenylalanine at the starter units (Miyanaga et al., 2016; Kudo et al., 2015). Hitachimycin and related compounds, such as vicenistatin, fluvirucin A1, fluvirucin B2, cremimycin, and incednine contained an aromatic ring of a β-amino acid as its polyketide skeleton. Hitachimycin has been reported to possess antiprotozoal and antitumor properties, but there a lack of literature on its antiviral effect. Fluvirucins, which have a core of macrocyclic lactam similar to hitachimycin, showed antiviral effects against influenza virus type A (Victoria strain) in MDCK cell culture, with IC_{50} = 2–10 μg/mL. It also showed low CC_{50} values, similar to those observed in our study (Naruse et al., 1991a, 1991b). The antimicrobial evidence indicated that polyketide synthase could synthesize each metabolite of hitachimycin and fluvirucins. Gene analysis and cluster study have been applied to identify the biosynthetic genes of the enzymes that contribute to biosynthetic machinery to develop new compounds (Kudo et al., 2015).

Two reference inhibitors, ribavirin, and lopinavir, were included in our experiments. Ribavirin is a synthetic nucleoside and a ribosyl purine analog with antiviral activity. The mechanism of action of ribavirin is still unclear and highly variable among patients (Cameron and Castro, 2001; Zumla et al., 2016). However, it from isolated is known to interfere with the synthesis of viral mRNA and viral replication, and is primarily indicated for hepatitis C virus (Dixit and Perelson, 2006). The activity of ribavirin is enhanced by using its combination with interferons or other antiviral drugs that synergistically inhibit the viruses, rather than treatment with ribavirin alone, as reported for the MERS-CoV and SARS-CoV regimens (Falzarano et al., 2013; Omrani et al., 2014). Ribavirin in combination with lopinavir/ritonavir and steroids showed a slight reduction in the mortality rate in patients infected with SARS-CoV (Chan et al., 2003). It has been used as a reference antiviral compound for testing the antiviral activities of candidate compounds in several studies. In our pre- and post-viral entry experiments, ribavirin showed less antiviral effect on FIPV, compared to compounds NSC345647, NSC87511, and NSC343256 (EC_{50} = 48.87–73.98 μM). Furthermore, it did not show an antiviral effect in the prophylaxis study.

Lopinavir, an inhibitor of HIV protease, has been commonly used in combination with ritonavir for treatment of HIV. The booted forms of lopinavir and ritonavir have exhibited antiviral activities in some clinical cases of MERS-CoV and SARS-CoV (Chu et al., 2004; Chan et al., 2003). It was expected that lopinavir could possibly inhibit 3CL^{pro} activity. However, lopinavir and its derivatives partially inhibited the 3CL^{pro} of SARS-CoV, with IC_{50} values of ~50 μM and ~25 μM, respectively (Wu et al., 2004). We observed that lopinavir effectively inhibited FIPV during the stage of viral entry (EC_{50} = 5.38–31.70 μM). It is possible that lopinavir may have higher inhibitory activity toward other proteases when examined by cell-based experiments. The papain-like protease 1 (PL1^{pro}), a common protease of CoV, has a finger-shaped subdomain and a catalytic triad Cys32–His183–Asp196, which have been found only in the alpha-CoV including FIPV, but absent in beta-CoV (Lei et al., 2018). For other host proteases such as furin protease, the action of lopinavir might involve the blocking of furin-mediated cleavage during viral entry. Therefore, the mechanism of

action of lopinavir on FIPV requires further investigation.

The selectivity index, defined as the ratio between CC_{50} and EC_{50}, was used to determine the drug selectivity. The cut-off value of SI for "hit" compounds set for this study was ≥ 4 (Severson et al., 2007). Our study showed that the SI value of NSC345647 in the pre-viral entry assay was 8.88. However, for the post-viral entry and prophylactic antiviral activity assays, it showed SI values of 2.20 and 3.69, respectively. The binding affinity of this compound to the binding pocket of FIPV $3CL^{pro}$ was determined as -8.3 kcal/mol using the program Autodock Vina. On the other hand, NSC87511 had SI values > 4 for all the three antiviral assays. Therefore, NSC345647 and NSC87511 were promising candidate natural compounds for drug development. Some inactive compounds CID5318214, CID3821945, CID5748601, and CID5372747 also inhibited protease activity, but could not control FIPV infection under all the tested conditions. It is possible that their anti-protease activities might be influenced by unknown factors within the cell-culture conditions, resulting in lower activity.

The three compounds (NSC345647, NSC87511, and NSC343256) with the EC_{50} values better than the broad spectrum antiviral drug, ribavirin, and the known viral protease inhibitor, lopinavir, were less effective when their activities were examined in the post-viral entry and prophylactic antiviral experiments (Table 1). In the case of post-viral entry, capability of the selected compounds to penetrate through the plasma membrane might be poor. Therefore, intracellular concentration of the compounds was less than the actual amount added in the culture media. For the prophylactic purpose, the compounds stability was very crucial. The antiviral activities of these compounds may be improved by utilizing a special drug delivery system that directs the compounds to macrophages and carries them inside the cells. Recently, nanoparticle-encapsulated drugs have been reported as a cargo for biopharmaceutical delivery to the target cells as well as preventing drug degradation (reviewed by Visser et al., 2019). On the other hand, modification by adding functional groups such as carboxyl, methyl, acetyl, aldehyde or ketone to the compound can improve their binding affinities, solubility or stability. However, the modification should not decrease their drug-like characteristics. In this study, we have modified the compound NSC87511 by adding a acetyl group as shown in Supplementary Table 3 which strengthened its interaction with the $3C^{pro}$ binding pocket and might enhance cell permeability.

FIPV $3CL^{pro}$ contains a Cys residue as the nucleophile of the catalytic dyad (St. John et al., 2015; Wang et al., 2015). Usually, the inhibitors of $3CL^{pro}$ are designed to facilitate the nucleophilic attack by protease at the carbonyl residue for the formation of a covalent bond with the inhibitor and trap the enzymatic nucleophile, terminating its catalytic activity. The functional groups are commonly termed as 'warheads', which are based on carbonyl groups and contain dipeptidyl residues with different warheads (Tiew et al., 2011; Kim et al.; 2012, 2013). The dipeptidyl aldehyde contains a carbonyl group with a nucleophile that can donate a pair of electrons. Consequently, hydrolysis of the key catalytic group occurs at the active site of $3CL^{pro}$. In this study, we observed that most of the candidate compounds contained an acyl group, which tends to share a lone-pair of electrons to the active site of FIPV $3CL^{pro}$. According to our molecular docking analysis, the three best candidate compounds interacted with the His41 or Cys144 and other residues in the binding pocket, mainly through non-covalent bonds. We also evaluated the ADME/T properties, which were useful in prioritizing drug modifications. We observed that NSC87511 and NSC343256 passed the Ro5 and had good 'drug-like' properties of small molecules for refinement into potential oral drugs. However, NSC345647 violated two of the Ro5 filters. Nevertheless, modification of the chemical structures should be able to reduce the undesirable properties and increase the drug-like fragment contents. In our study, the FIPV $3CL^{pro}$–compound complexes were mainly stabilized by the non-covalent interactions within the binding pocket. Therefore, besides the affinity of the molecule to its protein target, its chemical structure, especially the properties related to bioavailability and serum albumin binding, should be considered.

In conclusion, we utilized the application of computer-based assays for virtual screening to determine potential antiviral candidates for the treatment of FIP. We targeted the FIPV $3CL^{pro}$, which is responsible for poly-protein processing in CoV during viral replication. We identified three best candidate compounds that possessed the characteristics of antiviral inhibitors. These natural compounds showed strong affinity toward the target and inhibited the FIPV infection, as determined by molecular docking and cell-based assays.

Declaration of competing interest

None.

Acknowledgements

This work was supported by the Thailand Research Fund (grant numbers MRG6080067); Thailand Science Research and Innovation (grant number RTA6280011); Kasetsart Veterinary Development Funds, Thailand; and The New Southbound Policy and the Featured Areas Research Center Program within the framework of the Higher Education Sprout Project by the Ministry of Education in Taiwan. The authors thank Dr. Day-Yu Chao at National Chung Hsing University for assistance with protease inhibitory assay.

Appendix A. Supplementary data

Supplementary data to this article can be found online at https://doi.org/10.1016/j.antiviral.2019.104697.

References

Balzarini, J., Keyaerts, E., Vijgen, L., Vandermeer, F., Stevens, M., De Clercq, E., Egberink, H., Van Ranst, M., 2006. Pyridine N-oxide derivatives are inhibitory to the human SARS and feline infectious peritonitis coronavirus in cell culture. J. Antimicrob. Chemother. 57, 472–481. https://doi.org/10.1093/jac/dki481.

Berry, M., Fielding, B.C., Gamieldien, J., 2015. Potential broad spectrum inhibitors of the Coronavirus 3CLpro: a virtual screening and structure-based drug design study. Viruses 7, 6642–6660. https://doi.org/10.3390/v7122963.

Cameron, C.E., Castro, C., 2001. The mechanism of action of ribavirin: lethal mutagenesis of RNA virus genomes mediated by the viral RNA-dependent RNA polymerase. Curr. Opin. Infect. Dis. 14, 757–764. https://doi.org/10.1097/00001432-200112000-00015.

Chan, K.S., Lai, S.T., Chu, C.M., Tsui, E., Tam, C.Y., Wong, M.M.L., Tse, M.W., Que, T.L., Peiris, J.S.M., Sung, J., Wong, V.C.W., Yuen, K.Y., 2003. Treatment of severe acute respiratory syndrome with lopinavir/ritonavir: a multicentre retrospective matched cohort study. Hong Kong Med. J. 9, 399–406.

Chu, C.M., Cheng, V.C.C., Hung, I.F.N., Wong, M.M.L., Chan, K.H., Chan, K.S., Kao, R.Y.T., Poon, L.L.M., Wong, C.L.P., Guan, Y., Peiris, J.S.M., Yuen, K.Y., 2004. Role of lopinavir/ritonavir in the treatment of SARS: initial virological and clinical findings. Thorax 59, 252–256. https://doi.org/10.1136/thorax.2003.012658.

Daina, A., Michielin, O., Zoete, V., 2017. SwissADME: a free web tool to evaluate pharmacokinetics, drug-likeness and medicinal chemistry friendliness of small molecules. Sci. Rep. 7, 42717. https://doi.org/10.1038/srep42717.

Dallakyan, S., Olson, A.J., 2015. Small-molecule library screening by docking with PyRx. Methods Mol. Biol. 1263, 243–250. https://doi.org/10.1007/978-1-4939-2269-7.

Dixit, N.M., Perelson, A.S., 2006. The metabolism, pharmacokinetics and mechanisms of antiviral activity of ribavirin against hepatitis C virus. Cell. Mol. Life Sci. 63, 832–842. https://doi.org/10.1007/s00018-005-5455-y.

Falzarano, D., de Wit, E., Rasmussen, A.L., Feldmann, F., Okumura, A., Scott, D.P., Brining, D., Bushmaker, T., Martellaro, C., Baseler, L., Benecke, A.G., Katze, M.G., Munster, V.J., Feldmann, H., 2013. Treatment with interferon-α2b and ribavirin improves outcome in MERS-CoV–infected rhesus macaques. Nat. Med. 19, 1313. https://doi.org/10.1038/nm.3362.

Herrewegh, A.A.P.M., De Groot, R.J., Cepica, A., Egberink, H.F., Horzinek, M.C., Rottier, P.J.M., 1995. Detection of feline coronavirus RNA in feces, tissues, and body fluids of naturally infected cats by reverse transcriptase PCR. J. Clin. Microbiol. 33, 684–689. https://doi.org/10.1016/S0378-1135(98)00210-7.

Hsu, M.-F., Kuo, C.-J., Chang, K.-T., Chang, H.-C., Chou, C.-C., Ko, T.-P., Shr, H.-L., Chang, G.-G., Wang, A.H.-J., Liang, P.-H., 2005. Mechanism of the maturation process of SARS-CoV 3CL protease. J. Biol. Chem. 280, 31257–31266. https://doi.org/10.1074/JBC.M502577200.

Kim, Y., Mandadapu, S.R., Groutas, W.C., Chang, K.O., Mandadapu, S.R., Groutas, W.C., Chang, K.O., 2013. Potent inhibition of feline coronaviruses with peptidyl compounds targeting coronavirus 3C-like protease. Antivir. Res. 97, 161–168. https://doi.org/10.1016/j.antiviral.2012.11.005.

Kim, Y., Lovell, S., Tiew, K.-C., Mandadapu, S.R., Alliston, K.R., Battaile, K.P., Groutas,

W.C., Chang, K.-O., 2012. Broad-spectrum antivirals against 3C or 3C-like proteases of picornaviruses, noroviruses, and coronaviruses. J. Virol. 86, 11754–11762. https://doi.org/10.1128/JVI.01348-12.

Kudo, F., Kawamura, K., Uchino, A., Miyanaga, A., Takayanagi, R., Numakura, M., Eguchi, T., 2015. Genome mining of the hitachimycin biosynthetic gene cluster: involvement of a phenylalanine-2,3-aminomutase in biosynthesis. Chembiochem 16, 909–914. https://doi.org/10.1002/cbic.201500040.

Kuo, C.J., Chi, Y.H., Hsu, J.T.A., Liang, P.H., 2004. Characterization of SARS main protease and inhibitor assay using a fluorogenic substrate. Biochem. Biophys. Res. Commun. 318, 862–867. https://doi.org/10.1016/j.bbrc.2004.04.098.

Laskowski, R.A., Swindells, M.B., 2011. LigPlot+: multiple ligand-protein interaction diagrams for drug discovery. J. Chem. Inf. Model. 51, 2778–2786. https://doi.org/10.1021/ci200227u.

Lekcharoensuk, P., Wiriyarat, W., Petcharat, N., Lekcharoensuk, C., Auewarakul, P., Richt, J.A., 2012 Feb Feb. Cloned cDNA of A/swine/Iowa/15/1930 internal genes as a candidate backbone for reverse genetics vaccine against influenza A viruses. Vaccine 30, 1453–1459. https://doi.org/10.1016/j.vaccine.2011.12.109.

Lei, J., Kusov, Y., Hilgenfeld, R., 2018. Nsp3 of coronaviruses: structures and functions of a large multi-domain protein. Antivir. Res. 149, 58–74. https://doi.org/10.1016/j.antiviral.2017.11.001.

Lin, C.-N., Chang, R.-Y., Su, B.-L., Chueh, L.-L., 2013. Full genome analysis of a novel type II feline coronavirus NTU156. Virus Genes 46, 316–322. https://doi.org/10.1007/s11262-012-0864-0.

Lin, C.-W., Tsai, F.-J., Tsai, C.-H., Lai, C.-C., Wan, L., Ho, T.-Y., Hsieh, C.-C., Chao, P.-D.L., 2005. Anti-SARS coronavirus 3C-like protease effects of Isatis indigotica root and plant-derived phenolic compounds. Antivir. Res. 68, 36–42. https://doi.org/10.1016/J.ANTIVIRAL.2005.07.002.

Lipinski, C.A., 2004. Lead- and drug-like compounds: the rule-of-five revolution. Drug Discov. Today Technol. 1, 337–341. https://doi.org/10.1016/J.DDTEC.2004.11.007.

Lohézic-Le Dévéhat, F., Tomasi, S., Elix, J.A., Rouaud, I., Uriac, P., Rennes, D., Lohezic-Le Devehat, F., Tomasi, S., Elix, J.A., Bernard, A., Rouaud, I., Uriac, P., Boustie, J., 2007. Stictic acid derivatives from the lichen Usnea articulata and their antioxidant activities. J. Nat. Prod. 70, 1218–1220. https://doi.org/10.1021/np070145k.

Manasateinkij, W., Nilkumhang, P., Jaroensong, T., Noosud, J., Lekcharoensuk, C., Lekcharoensuk, P., 2009. Occurrence of feline coronavirus and feline infectious peritonitis virus in Thailand. Kasetsart J./Nat. Sci. 43, 720–726.

Miyanaga, A., Hayakawa, Y., Numakura, M., Hashimoto, J., Teruya, K., Hirano, T., Shin-Ya, K., Kudo, F., Eguchi, T., 2016. Identification of the fluvirucin B2(Sch 38518) biosynthetic gene cluster from actinomadura fulva sub sp. Indica ATCC 53714: substrate Specificity of the β-amino acid selective adenylating enzyme FlvN. Biosci. Biotechnol. Biochem. 80, 935–941. https://doi.org/10.1080/09168451.2015.1132155.

Naruse, N., Tenmyo, O., Kawano, K., Tomita, K., Ohgusa, N., Miyaki, T., Konishi, M., Oki, Toshikazu, 1991a. Fluvirucins A1, A2, B1, B2, B3, B4 and B5, new antibiotics active against influenza a virus. I. production, isolation, chemical properties, and biological activities. J. Antibiot. (Tokyo) 44, 733–740. https://doi.org/10.7164/antibiotics.44.733.

Naruse, N., Konishi, M., Oki, T., Inouye, Y., Kakisawa, H., 1991b. Fluvirucins A1, A2, B1, B2, B3, B4 and B5, new antibiotics active against influenza a virus. III. The stereochemistry and absolute configuration of fluvirucin A1. J. Antibiot. (Tokyo) 44, 756–761. https://doi.org/10.7164/antibiotics.44.756.

Neamati, N., Hong, H., Mazumder, A., Wang, S., Sunder, S., Nicklaus, M.C., Milne, G.W.A., Proksa, B., Pommier, Y., 1997. Depsides and depsidones as inhibitors of HIV-1 integrase: discovery of novel inhibitors through 3D database searching. J. Med. Chem. 40, 942–951. https://doi.org/10.1021/jm960759e.

Omer, A., Singh, P., 2017. An integrated approach of network-based systems biology, molecular docking, and molecular dynamics approach to unravel the role of existing antiviral molecules against AIDS-associated cancer. J. Biomol. Struct. Dyn. 35, 1547–1558. https://doi.org/10.1080/07391102.2016.1188417.

Omrani, A.S., Saad, M.M., Baig, K., Bahloul, A., Abdul-Matin, M., Alaidaroos, A.Y., Almakhlafi, G.A., Albarrak, M.M., Memish, Z.A., Albarrak, A.M., 2014. Ribavirin and interferon alfa-2a for severe Middle East respiratory syndrome coronavirus infection: a retrospective cohort study. Lancet Infect. Dis. 14, 1090–1095. https://doi.org/10.1016/S1473-3099(14)70920-X.

Papadopoulou, P., Tzakou, O., Vagias, C., Kefalas, P., Roussis, V., 2007. β-Orcinol metabolites from the lichen *Hypotrachyna revoluta*. Molecules. https://doi.org/10.3390/12050997.

Pedersen, N.C., 2014a. An update on feline infectious peritonitis: virology and immunopathogenesis. Vet. J. 201, 123–132. https://doi.org/10.1016/j.tvjl.2014.04.017.

Pedersen, N.C., 2014b. An update on feline infectious peritonitis: diagnostics and therapeutics. Vet. J. 201, 133–141. https://doi.org/10.1016/j.tvjl.2014.04.016.

Pedersen, N.C., 2009. A review of feline infectious peritonitis virus infection: 1963-2008. J. Feline Med. Surg. 11, 225–258. https://doi.org/10.1016/j.jfms.2008.09.008.

Ryu, Y.B., Jeong, H.J., Kim, J.H., Kim, Y.M., Park, J.-Y., Kim, D., Naguyen, T.T.H., Park, S.-J., Chang, J.S., Park, K.H., Rho, M.-C., Lee, W.S., 2010. Biflavonoids from *Torreya nucifera* displaying SARS-CoV $3CL^{pro}$ inhibition. Bioorg. Med. Chem. 18, 7940–7947. https://doi.org/10.1016/J.BMC.2010.09.035.

Sander, T., Freyss, J., von Korff, M., Rufener, C., 2015. DataWarrior: an open-source program for chemistry aware data visualization and analysis. J. Chem. Inf. Model. 55 (2), 460–473. https://doi.org/10.1021/ci500588j.

Severson, W.E., Shindo, N., Sosa, M., Fletcher, T., White, E.L., Ananthan, S., Jonsson, C.B., 2007. Development and validation of a high-throughput screen for inhibitors of SARS CoV and its application in screening of a 100,000-compound library. J. Biomol. Screen 12, 33–40. https://doi.org/10.1177/1087057106296688.

Singh, S.B., Zink, D.L., Bills, G.F., Teran, A., Silverman, K.C., Lingham, R.B., Felock, P., Hazuda, D.J., 2003. Four novel bis-(naphtho-γ-pyrones) isolated from *Fusarium* species as inhibitors of HIV-1 integrase. Bioorg. Med. Chem. Lett 13, 713–717. https://doi.org/10.1016/S0960-894X(02)01057-0.

St John, S.E., Therkelsen, M.D., Nyalapatla, P.R., Osswald, H.L., Ghosh, A.K., Mesecar, A.D., 2015. X-ray structure and inhibition of the feline infectious peritonitis virus 3C-like protease: structural implications for drug design. Bioorg. Med. Chem. Lett 25, 5072–5077. https://doi.org/10.1016/j.bmcl.2015.10.023.

Tiew, K.C., He, G., Aravapalli, S., Mandadapu, S.R., Gunnam, M.R., Alliston, K.R., Lushington, G.H., Kim, Y., Chang, K.O., Groutas, W.C., 2011. Design, synthesis, and evaluation of inhibitors of Norwalk virus 3C protease. Bioorg. Med. Chem. Lett 21, 5315–5319. https://doi.org/10.1016/j.bmcl.2011.07.016.

Trott, O., Olson, A.J., 2010. AutoDock Vina: improving the speed and accuracy of docking with a new scoring function, efficient optimization, and multithreading. J. Comput. Chem. 31, 455–461. https://doi.org/10.1002/jcc.21334.

Umezawa, I., Takeshima, H., Komiyama, K., Koh, Y., Yamamoto, H., Kawaguchi, M., 1981. A new antitumor antibiotic, stubomycin. J. Antibiot. (Tokyo) 34, 259–265. https://doi.org/10.7164/antibiotics.34.259.

Ugaki, N., Yamazaki, H., Uchida, R., Tomoda, H., 2012. New isochaetochromin, an inhibitor of triacylglycerol synthesis in mammalian cells, produced by *Penicillium* sp. FKI-4942: II. structure elucidation. J. Antibiot. (Tokyo) 65, 21–24. https://doi.org/10.1038/ja.2011.106.

Visser, J.G., Van Staden, A.D.P., Smith, C., 2019. Harnessing macrophages for controlled-release drug delivery: lessons from microbes. Front. Pharmacol. 9, 1–18. https://doi.org/10.3389/fphar.2019.00022.

Vu, T.H., Lamer, A.C. Le, Lalli, C., Samson, J.B.M., Dévéhat, F.L., Le Seyec, J.Le, 2015. Depsides: lichen metabolites active against hepatitis C virus. PLoS One 10, 1–14. https://doi.org/10.1371/journal.pone.0120405.

Wang, F., Chen, C., Liu, X., Yang, K., Xu, X., Yang, H., 2015. Crystal structure of feline infectious peritonitis virus main protease in complex with synergetic dual inhibitors. J. Virol. 90, 1910–1917. https://doi.org/10.1128/JVI.02685-15.

Wassman, C.D., Baronio, R., Demir, Ö., Wallentine, B.D., Chen, C.K., Hall, L.V., Salehi, F., Lin, D.W., Chung, B.P., Wesley Hatfield, G., Richard Chamberlin, A., Luecke, H., Lathrop, R.H., Kaiser, P., Amaro, R.E., 2013. Computational identification of a transiently open L1/S3 pocket for reactivation of mutant p53. Nat. Commun. 4, 1–9. https://doi.org/10.1038/ncomms2361.

White, P.A., Oliveira, R., Araújo, A., Serafini, M., Moreira, J., Almeida, J., Oliveira, A., Santos, M., White, P., Quintans, J., Quintans-Junior, L., Gelain, D., 2014. Antioxidant activity and mechanisms of action of natural compounds isolated from lichens: a systematic review. Molecules 19, 14496–14527. https://doi.org/10.3390/molecules190914496.

Wu, C.-Y., Jan, J.-T., Ma, S., Kuo, C.-J., Juan, H.-F., Cheng, Y.-S.E., Hsu, H.-H., Huang, H.-C., Wu, D., Brik, A., Liang, F.-S., Liu, R.-S., Fang, J.-M., Chen, S.-T., Liang, P.-H., Wong, C.-H., 2004. Small molecules targeting severe acute respiratory syndrome human coronavirus. Proc. Natl. Acad. Sci. 101, 10012–10017. https://doi.org/10.1073/pnas.0403596101.

Zumla, A., Chan, J.F.W., Azhar, E.I., Hui, D.S.C., Yuen, K.Y., 2016. Coronaviruses-drug discovery and therapeutic options. Nat. Rev. Drug Discov. https://doi.org/10.1038/nrd.2015.37.